JACS
JOURNAL OF THE AMERICAN CHEMICAL SOCIETY

Article

pubs.acs.org/JACS

Experimental and Computational Study of BODIPY Dye-Labeled Cavitand Dynamics

Igor Pochorovski,[†] Tim Knehans,[‡] Daniel Nettels,[‡] Astrid M. Müller,[§] W. Bernd Schweizer,[†] Amedeo Caflisch,*[,‡] Benjamin Schuler,*[,‡] and François Diederich*[,†]

[†]Laboratorium für Organische Chemie, ETH Zürich, Hönggerberg, HCI, 8093 Zürich, Switzerland

[‡]Biochemisches Institut, Universität Zürich, Winterthurerstrasse 190, 8057 Zürich, Switzerland

[§]Beckman Institute, and Division of Chemistry and Chemical Engineering, California Institute of Technology, M/C 139-74, Pasadena, California 91125, United States

Supporting Information

ABSTRACT: Understanding the distance distribution and dynamics between moieties attached to the walls of a resorcin[4]arene cavitand, which is switchable between an expanded kite and a contracted vase form, might enable the use of this molecular system for the study of fundamental distance-dependent interactions. Toward this goal, a combined experimental and molecular dynamics (MD) simulation study on donor/acceptor borondipyrromethene (BODIPY) dye-labeled cavitands present in the vase and kite forms was performed. Direct comparison between anisotropy decays calculated from MD simulations with experimental fluorescence anisotropy data showed excellent agreement, indicating that the simulations provide an accurate representation of the dynamics of the system. Distance distributions between the BODIPY dyes were established by comparing time-resolved Förster resonance energy transfer experiments and MD simulations. Fluorescence intensity decay curves emulated on the basis of the MD trajectories showed good agreement with the experimental data, suggesting that the simulations present an accurate picture of the distance distributions and dynamics in this molecular system and provide an important tool for understanding the behavior of extended molecular systems and designing future applications.

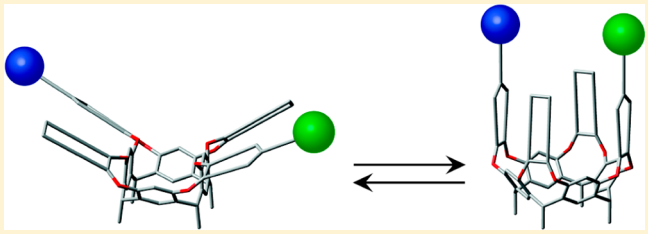

INTRODUCTION

Resorcin[4]arene cavitands are a fascinating switching platform because of their ability to adopt two spatially well-defined conformations: an expanded kite and a contracted vase. Switching the conformational and binding properties of cavitands has been achieved with a variety of stimuli, such as changes in temperature,[1] pH,[2] metal ion concentration,[3] light irradiation,[4] solvent,[5] and redox state.[6] Besides employing conformational switching of resorcin[4]arene cavitands as a means to change their binding properties, the cavitand system could eventually be used as a platform to investigate fundamental interactions between objects attached to the cavitand's walls with respect to their variable distance. The development of such molecular machines able to controllably perform mechanical motions involving large spatial rearrangements is a long-standing goal.[7] The cavitand system could be used for this purpose if the distance distribution and dynamics between objects connected to the cavitand can be precisely determined in both the vase and kite conformations.

We had set out toward this goal by preparing a donor–acceptor borondipyrromethene (BODIPY) dye-substituted cavitand **1a** (Chart 1), present in the vase form, for Förster resonance energy transfer (FRET)[8] studies.[7c,9] Surprisingly, an unexpectedly low FRET efficiency was observed already in the vase form (ca. 66%), although an efficiency close to 100% was expected assuming a close dye–dye distance of ca. 1 nm. Such distance would prevail if the cavitand arms were oriented parallel to one another, i.e., the average opening angle of the cavitand walls would be 0°. The low FRET efficiency was attributed to either dynamic behavior of the cavitand or an unfavorable orientation of the transition dipole moments of the dyes.[7c,9] To gain more insights into this problem, cavitand **1a** was resynthesized together with the analogous cavitands with shorter phenylene–ethynylene linkers, **1b** and **1c**.[10] As the FRET efficiencies increased toward cavitands with shorter linkers (in the series **1a**, **1b**, **1c**), it was concluded that the two arms of the cavitands are separated by a certain average opening angle and are not aligned parallel. Thereby, an average opening angle of 16° was inferred to explain the observed FRET efficiencies.[10]

In this work, we sought to gain detailed insights into the distance distribution and dynamics of the cavitand system in both the vase and the kite conformations. Toward this goal, we prepared BODIPY dye-labeled quinone-based cavitand **2** (Chart 1) that is present in the kite form (designed based on

Received: October 16, 2013
Published: February 3, 2014

   dx.doi.org/10.1021/ja4104292 | J. Am. Chem. Soc. 2014, 136, 2441–2449

Chart 1. Structures of Vase Cavitands 1a–d, Kite Cavitand 2, and Donor-Only Substituted Reference Cavitand 3

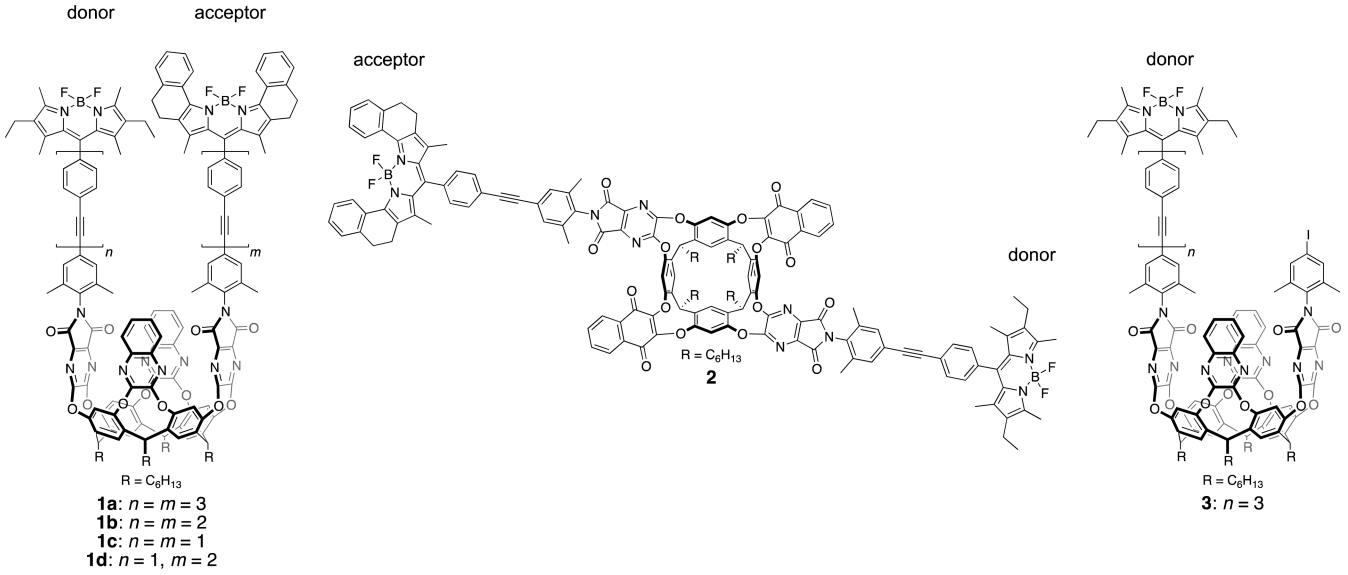

what we learned about conformational properties of diquinone–diquinoxaline cavitands).[5,6] In addition, we expanded the BODIPY dye-labeled cavitand vase series **1a–c** by cavitand **1d** featuring phenylene–ethynylene linkers of different lengths. Together, systems **1a–d** and **2** embody the two conformational extremes of cavitands and are therefore ideally suited for the projected investigation. We investigated the BODIPY dye-labeled cavitands in a combined experimental and theoretical study consisting of time-resolved fluorescence spectroscopy and molecular dynamics (MD) simulations. BODIPY donor dye-substituted cavitand **3** shown in Chart 1 served as a reference compound for fluorescence studies. MD simulations complemented the experimental results and yielded theoretical dye–dye distance distributions. Emulation of fluorescence decay curves based on the distance distributions obtained by MD simulations allowed direct comparison of experimental and theoretical results. This work not only provides insights into the conformational dynamics of cavitands but also serves as a case study for the interplay between time-resolved fluorescence spectroscopy and MD simulations—a combination of methods that is often used to investigate the dynamics of biological macromolecules[11]—applied to a relatively simple artificial small molecule system.

RESULTS AND DISCUSSION

Synthesis and Characterization. The synthesis of cavitands **1a–c** and **3** had been recently reported.[10] The synthesis and characterization of the newly prepared cavitands **1d** and **2** is described in section 1 of the Supporting Information.

Cavitands **1a–d** and **2** differ in that **1a–d** possess two quinoxaline walls, while **2** is equipped with two quinone walls. This small structural difference has a dramatic effect on cavitand conformation:[5] cavitands **1a–c** are present in the vase form (^{1}H NMR methine proton shifts at 5.61 and 5.69 ppm),[1,12] while cavitand **2** adopts the kite form (methine protons at 3.69 and 4.35 ppm) in $CDCl_3$ solution.

^{19}F NMR spectroscopy employing a pulse sequence with a 30° flip angle enabled determination of the BODIPY dye donor/acceptor ratios in cavitands **1a–d** and **2** based on the integral ratios of the respective BF_2 units. In cavitand **1a** this ratio was 1.00/0.82, corresponding to a donor-only fraction of 18%. In cavitand **1b** the donor-only fraction was 11%. On the other hand, in cavitands **1c**, **1d**, and **2**, the donor-only fractions were below the sensitivity limit of the NMR measurements (~2%). A possible explanation for higher ratios between donor/acceptor F atoms could be partial loss of the BF_2 units of the acceptor dyes during the course of cavitand syntheses, resulting in mixtures of fully labeled cavitands and cavitands lacking the BF_2 unit on the acceptor dyes.[13] Loss of the BF_2 unit in BODIPY dyes has precedence and was observed in high acidity media[14] or under strongly basic conditions,[15] and the corresponding products have been shown to be nonfluorescent.[14] Nevertheless, this finding is unexpected and has important implications for fluorescence studies, since the emission from this fraction of donor-only molecules needs to be taken into account for analysis of the fluorescence emission data.

X-ray Analysis. The X-ray structures of the precursors of cavitands **1a–d** and **2** and diiodocavitands **4**[16] and **5**[17] are shown in Figure 1. The solid-state conformational properties of the diiodocavitands are reflected by their solution-state properties: compound **4** crystallized in the vase form from $(CH_3)_2CO/CH_2Cl_2$, while compound **5** crystallized in the kite form from $CDCl_3$. While in cavitand **4** the I-bearing carbon atoms are placed at a distance of 0.86 nm to one another, in cavitand **5** the corresponding distance is 2.39 nm, which is almost 3 times larger.

Absorption and Steady-State Fluorescence Spectroscopy. The absorption and steady-state fluorescence spectra of cavitands **1a–d** and **2** are depicted in Figure 2 (top and bottom, respectively). The absorption spectra exhibit two main absorption bands corresponding to the donor dye moieties (λ_{max} = 529 nm) and the acceptor dye moieties (λ_{max} = 619 nm). The fluorescence spectra were recorded using an excitation wavelength of λ_{exc} = 490 nm; direct excitation of the acceptor is negligible at this wavelength.[18] The emission maxima at λ_{max} = 542 nm (I_{DA}) stem from the donor and at λ_{max} = 630 nm from the acceptor (I_{AD}) dye moieties. The intensity scale is referenced relative to the intensity maximum I_D of donor-only substituted cavitand **3**. The FRET efficiencies can be estimated according to eq 1

dx.doi.org/10.1021/ja4104292 | J. Am. Chem. Soc. 2014, 136, 2441–2449

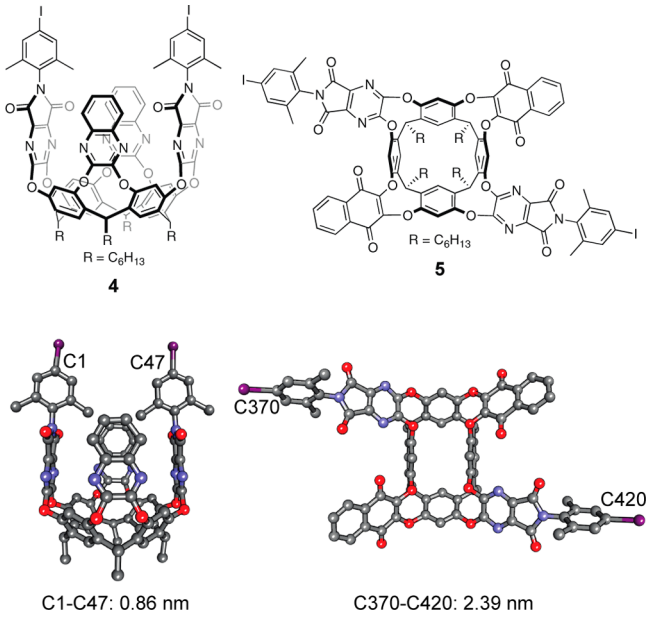

Figure 1. Molecular structures of **4**[16] (at 123 K) and **5** (at 100 K) in the crystals. Crystals of **4** and **5** were obtained by evaporation from $(CH_3)_2CO/CH_2Cl_2$ and $CDCl_3$, respectively. Solvent molecules, *n*-hexyl chains, and hydrogen atoms are omitted for clarity.

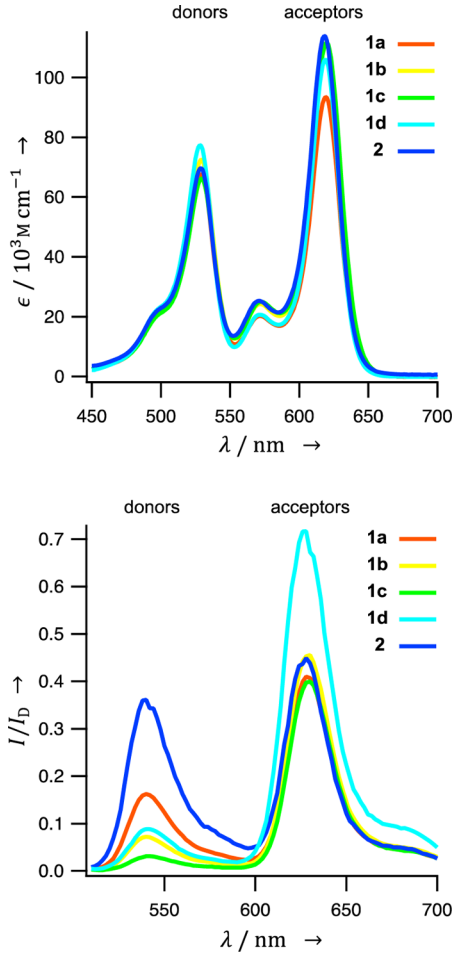

Figure 2. Absorption (top) and fluorescence emission (bottom, $c = 0.5 \times 10^{-7}$ M, λ_{exc} = 490 nm, I_D is the emission maximum of reference donor dye cavitand **3**) spectra of cavitands **1a–d** and **2** in $CDCl_3$.

$$E = 1 - \frac{I_{DA}}{I_D} \quad (1)$$

Higher FRET efficiencies are expected for shorter dye–dye distances. Consequently, cavitand **2**, which is present in the kite conformation, exhibits the lowest FRET efficiency (64%) among the five cavitands. On the other hand, vase cavitands **1a–d** exhibit *E* values ranging from 84% to 97% with smaller values for cavitands with longer arms. While these efficiencies are higher than in cavitand **2**, suggesting shorter dye–dye distances, they are not consistent with the assumption of parallel oriented cavitand walls found in X-ray structures, in which case FRET efficiencies of over 99% would be expected. This trend was originally explained with the presence of a cavitand opening angle of ca. 16°.[10] In light of the above-mentioned finding based on NMR that samples of cavitands with longer arms possess significant donor-only labeled fractions (18% and 11% for cavitands **1a** and **1b**, respectively), the increasing donor fluorescence intensity for cavitands with longer arms could also be explained by residual fluorescence stemming from these contributions. This interpretation is supported by fluorescence lifetime measurements, where the contribution of doubly and singly labeled molecules can be resolved more easily.

Time-Resolved Fluorescence Spectroscopy. We recorded donor and acceptor fluorescence decay curves using time-correlated single-photon counting after pulsed excitation of the donor dye at λ_{exc} = 470 nm for each sample containing cavitands **1a–d** and **2** (Figure 3) at concentrations of ca. 10^{-6} M in $CHCl_3$. For a pure sample of donor–acceptor-labeled species with a single fixed distance, one expects to measure single-exponential donor fluorescence decays with a mean fluorescence lifetime τ_{DA} reduced by a factor of $(1 - E)$ as compared to the mean donor fluorescence lifetime τ_D obtained in the absence of the acceptor. Further, the acceptor decay curve should exhibit an initial rise (with rate constant $1/\tau_{DA}$) due to the FRET-induced population of the acceptor excited state and a subsequent single-exponential decay with $1/\tau_A$, where τ_A is the mean fluorescence lifetime of the acceptor dye.[19] This behavior is clearly observed for the kite cavitand **2**. The corresponding donor decay curve was fitted with a single-exponential decay convolved with the instrument response function (IRF), yielding τ_{DA} = 1.51 ns. This value results in a mean FRET efficiency of 64% (using τ_D = 4.21 ns of reference cavitand **3** that is lacking the acceptor dye),[20] which is in excellent agreement with the steady-state fluorescence spectroscopy data. Note, however, that obtaining accurate distance information from this value requires the distance distribution and dynamics of the system to be taken into account.

The acceptor decay curves of vase cavitands **1a–d** are virtually identical and identical to the decay curve of the acceptor in **1a** directly excited with τ_{exc} = 582 nm.[20] Their steep initial rise, which occurs within the response time of the instrument, shows that the FRET efficiencies in cavitands **1a–d** are near 100% and donor and acceptor dyes thus in very close proximity. The fluorescence emission of the donor is thus expected to be very weak, and the corresponding donor fluorescence lifetimes are very short. Note, however, that monitoring the sensitized acceptor emission has the advantage that only signal from molecules containing both a donor and an intact acceptor fluorophore is detected. In contrast, the fluorescence emission from the donor contains the signal of molecules lacking an active acceptor, whose presence we

dx.doi.org/10.1021/ja4104292 | J. Am. Chem. Soc. 2014, 136, 2441–2449

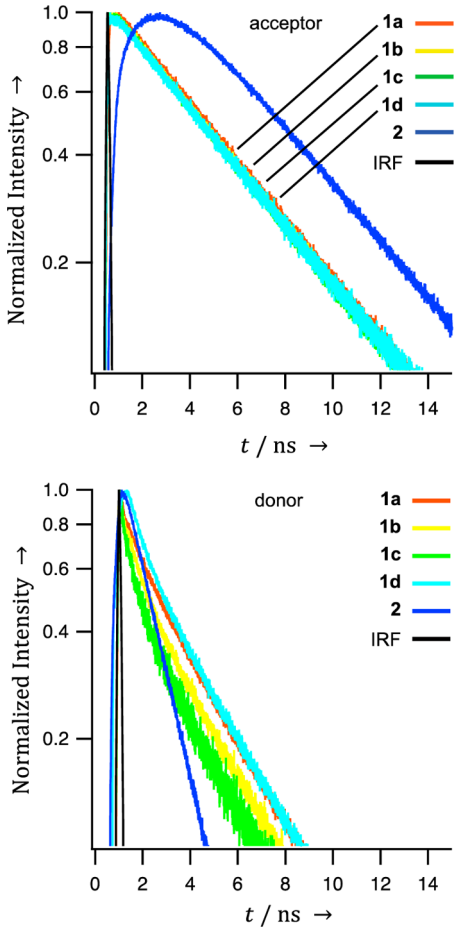

Figure 3. Fluorescence decay curves of the acceptor (top) and donor (bottom) moieties of cavitands **1a–d** and **2**. Measurements were performed under magic angle configuration, i.e., with the emission polarizer set to 54.7° with respect to the excitation polarization. IRF = Instrument response function.

quantified using NMR spectroscopy (see Synthesis and Characterization). The residual donor fluorescence intensity decays of cavitands **1a–d** (Figure 3b) are thus dominated by the emission from these donor-only molecules. As a result, they exhibit decay components up to the lifetime of the isolated donor fluorophore in the range of 4 ns[21] but also additional shorter lifetime components, presumably because of collisional quenching with the acceptor moiety lacking the BF_2 unit. Such multiexponential behavior is typical of BODIPY dye dimers or BODIPY dyes in confined environments (in proteins, lipids, micelles, or glasses).[22]

MD Simulations. To obtain a detailed molecular picture of the dye–dye distance distributions and dynamics underlying the fluorescence results, we performed MD simulations with explicit chloroform solvent for cavitands **1a–d** and **2**. For direct comparison to the experimental data and benchmarking of the MD results, we calculated observable properties such as fluorescence intensity and fluorescence anisotropy decay curves from the MD trajectories. Reports on MD simulations of supramolecular systems in explicit solvents are rare.[23] One reason for this is that early force fields were designed to simulate biomolecules in aqueous media. Recently, all-atom general force fields[24] and tools for automatic parameter assignment[24a,25] have been developed, as well as structure and topology files for various common organic solvents.[26] One goal of our study was therefore to utilize these developments and to investigate the applicability of MD simulations to molecular and supramolecular chemistry. The most common general force fields employed in contemporary MD literature are the General AMBER Force Field (GAFF)[24a] and the CHARMM General Force Field (CGenFF).[24b] For comparison, we included both force fields in our study.[27]

The most critical aspect in modeling cavitands **1a–d** and **2** are the phenylene–ethynylene linkers; small errors in their force field parameters would propagate to larger errors in BODIPY dye–dye distances. A common parameter in describing the stiffness of linker units is the persistence length L_p, whereby larger L_p values represent stiffer linkers. The persistence length of the phenylene–ethynylene unit had been recently experimentally determined on the basis of pulse electron paramagnetic resonance (EPR) spectroscopy on spin-labeled test systems.[28] We subjected these phenylene–ethynylene-containing systems (see the Supporting Information, section 6) to MD simulations with CGenFF and GAFF (explicit chloroform, 100 ns each) to investigate how well the two force fields reproduce the experimentally determined L_p value. Values of L_p = 18.4 ± 2.2 nm for CGenFF and L_p = 27.0 ± 2.4 nm for GAFF were obtained. Comparison to the experimental value of L_p = 13.8 ± 1.5 nm[28] suggests that both force fields slightly overestimate the rigidity of the oligo(phenylene–ethynylene) linker, but especially the results from CGenFF provide reasonably good agreement.

The cavitands **1a–d** and **2** were subjected to MD simulations with the force fields CGenFF and GAFF (explicit chloroform, 500 ns each). The resulting BODIPY dye–dye distance histograms are illustrated in Figure 4. For the vase cavitands **1a–d**, both force fields yield histograms composed of sharp maxima at ca. 0.5 and 1.0 nm and broader distributions spanning from 0.5 to 1.9 nm in the case of the smallest cavitand **1c** and from 0.5 to 3.0 nm in the case of the largest cavitand **1a**. While the sharp maxima can be ascribed to arrangements where the BODIPY dyes are in direct contact, the broader distributions are due to motions of separated dyes.

On the other hand, the kite cavitand **2** yields single-distribution histograms spanning from 3.0 to 5.0 nm. The mean dye–dye distances $\langle d(B\cdots B)\rangle$ obtained with the two force fields differ only marginally. The MD simulations slightly underestimate the average opening angle of cavitand **2**, as evidenced by comparing the C370–C420 distance (Figure 1) in the X-ray structure of cavitand **5** (2.39 nm) with the corresponding average C–C distance stemming from the CGenFF simulation of cavitand **2** (2.33 nm). If this discrepancy of 0.06 nm is propagated toward the BODIPY dyes, a small deviation of ca. 0.1 nm for the average simulated dye–dye distance can be expected.

Notably, there is no overlap between the dye–dye distance distributions of vase cavitand **1c** and kite cavitand **2**, which have the same linker length. Thus, switching between both cavitand conformations can entirely change the distance distribution profile of moieties attached to the cavitand walls.

Distance Autocorrelation from MD Data. To determine the time scale on which the distance dynamics of the BODIPY dye arms relative to each other takes place, we calculated the time-correlation functions[29]

$$g(\tau) = \frac{\langle R(t+\tau)R(t)\rangle_t}{\langle R(t)\rangle_t^2} \quad (2)$$

dx.doi.org/10.1021/ja4104292 | J. Am. Chem. Soc. 2014, 136, 2441–2449

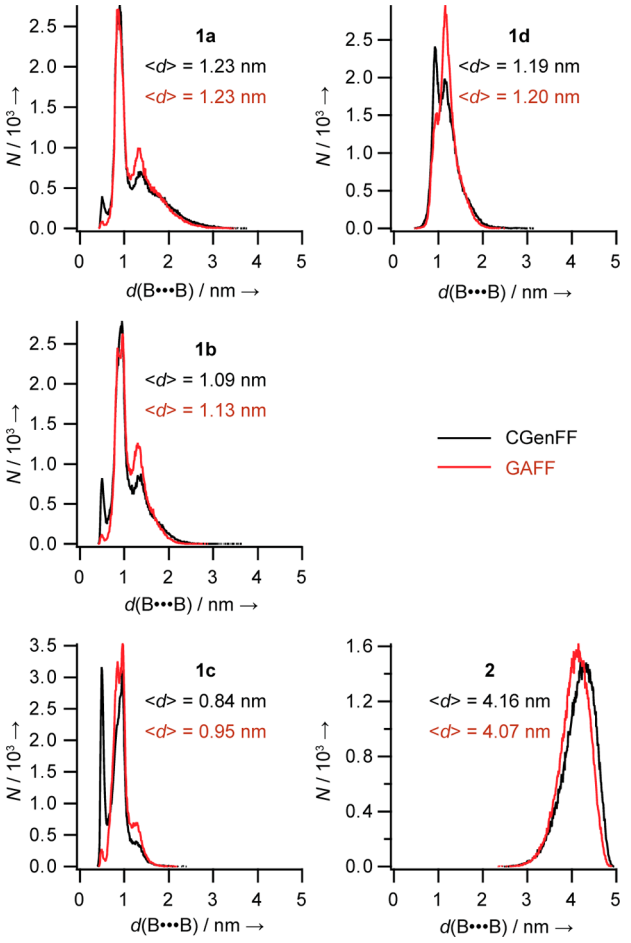

Figure 4. Histograms of distances between the B atoms of the donor and acceptor BODIPY dyes of cavitands **1a**–**d** and **2**, simulated with CGenFF (black) and GAFF (red).

from the CGenFF-simulated interdye distance data of cavitands **1a** and **2** (Figure 5); $R(t)$ is the dye–dye distance d(B···B) at time t, $\langle ... \rangle_t$ denotes the time average over t, and τ is the lag time. The results show that the interdye distance dynamics of both cavitands occur on a subnanosecond time scale, with the dynamics of vase cavitand **1a** being slower than those of kite cavitand **2** by almost an order of magnitude. This finding is

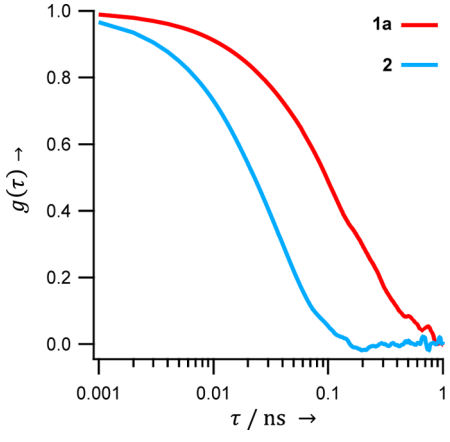

Figure 5. Autocorrelation functions of the interdye distances derived from CGenFF-MD simulations of cavitands **1a** and **2**.

presumably due to a slow down of the distance dynamics in cavitand **1a** caused by dye–dye contacts in the closed conformation.

Fluorescence Anisotropy. A stringent way of testing the accuracy of the time scales of dynamics in the simulations, including the viscosity of the solvent, is direct comparison to fluorescence anisotropy data. Anisotropy decays report on rotational diffusion times of the entire cavitands as well as on segmental rotation times of the BODIPY dye arms.[30] We measured the anisotropy decay of the acceptor dye of cavitand **1a** and compared it to the expected anisotropy decay as calculated from the corresponding MD simulations.

Fluorescence anisotropy decays were obtained by measuring the fluorescence intensity decays $I_{VV}(t)$ and $I_{VH}(t)$ observed after pulsed excitation of the acceptor dye (λ_{exc} = 582 nm); in both measurements the plane of the linear polarized excitation light was vertically oriented and the emission polarizer was set vertically for I_{VV} and horizontally for I_{VH} (Figure 6, top). We fitted the two curves globally with model curves $I_{\parallel}$ and $I_{\perp}$

$$I_{\parallel} = I_0(1 + 2r(t))e^{-t/\tau_A} \quad (3)$$

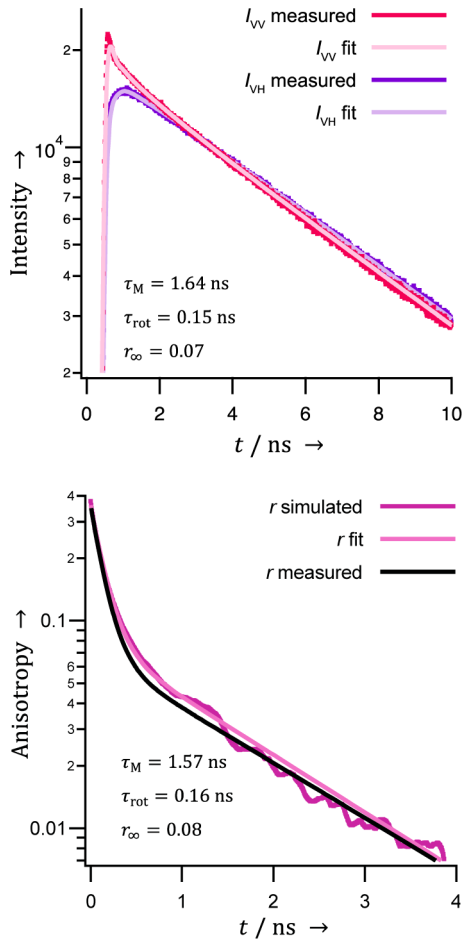

Figure 6. (Top) Acceptor fluorescence intensity decay curves of cavitand **1a** measured after acceptor excitation with λ_{exc} = 582 nm. I_{VV} was recorded with an emission polarization filter set to 0° and I_{VH} to 90° with respect to excitation polarization. (Bottom) Fluorescence anisotropy decay curves constructed from CGenFF-MD trajectory of cavitand **1a** using eq 6, fitted by the model described by eq 5, and the curve resulting from measured data inserted in eq 5.

dx.doi.org/10.1021/ja4104292 | J. Am. Chem. Soc. 2014, 136, 2441–2449

$$I_{\perp} = I_0(1 - r(t))e^{-t/\tau_A} \quad (4)$$

τ_A is the mean fluorescence lifetime of the acceptor dye and was determined to be τ_A = 5.24 ns.[20] $I_{\parallel}$ and $I_{\perp}$ were convolved with the IRF to yield I_{VV} = IRF⊗$I_{\parallel}$ and I_{VH} = G·IRF⊗$I_{\perp}$. The factor G describes the relative difference in detection efficiencies of vertical and horizontal polarized photons of the instrumentation.[30] For our instrument, we determined G = 1.1. The fluorescence anisotropy decay is defined as $r(t) = (I_{\parallel} - I_{\perp})/(I_{\parallel} + 2I_{\perp})$. We expected $r(t)$ to decay with two decay times: one corresponding to the overall rotational diffusion of the whole cavitand (τ_M), and the other corresponding to the rotational motion of the BODIPY dye relative to the cavitand (τ_{rot}). Hence, the anisotropy decay was described according to[31]

$$r(t) = ((r_0 - r_\infty)e^{-t/\tau_{rot}} + r_\infty)e^{-t/\tau_M} \quad (5)$$

where r_0 is the limiting anisotropy, which was fixed to 0.37,[22a] and r_∞ is the residual anisotropy. Fitting the intensity decays (Figure 6, top) yielded τ_M = 1.64 ns, τ_{rot} = 0.15 ns, and r_∞ = 0.07.

For direct comparison, we determined $r(t)$ also from the MD simulation of cavitand **1a**. The time trajectory of the normalized orientation vector $\vec{A}(t)$ of the acceptor dye was used to obtain the anisotropy decay according to[31]

$$r(t) = r_0\langle P_2(\vec{A}(t')\cdot\vec{A}(t' + t))\rangle_{t'} \quad (6)$$

Here, $P_2(x) = (3x^2 - 1)/2$ is the second Legendre polynomial and vector $\vec{A}$ is defined as indicated in Figure 7. We fitted the resulting anisotropy decay by eq 5 and obtained τ_M = 1.57 ns, τ_{rot} = 0.16 ns, and r_∞ = 0.08 (Figure 6, bottom). The excellent agreement between these values and the ones obtained from experimental anisotropy decay measurements provides good evidence that the MD simulations accurately capture the dynamics of the cavitands, including the effect of solvent and viscosity. The MD simulations should thus also be able to provide accurate insights in the combined effects of distance distributions and dynamics on the experimentally observed fluorescence intensity decays.

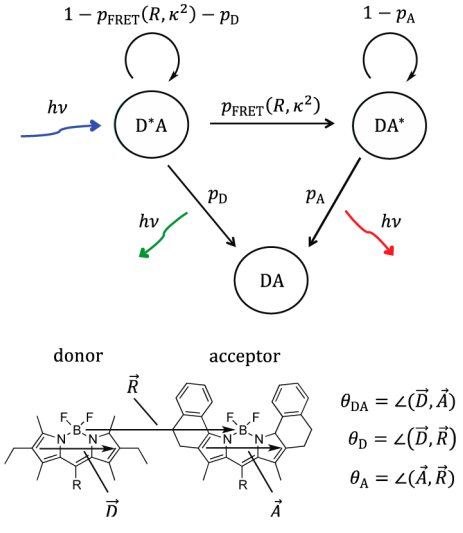

Figure 7. (Top) Markov chain model devised to emulate donor- and acceptor-fluorescence decay curves from simulated MD trajectories. (Bottom) Description of vectors and angles used for calculating κ^2 according to eq 12.

Fluorescence Decay Curves from MD Data. To enable a direct comparison of the simulations to the experimental data, we emulated donor fluorescence decay curves that would be expected on the basis of the CGenFF-simulated MD trajectories by taking into account the dye−dye distance and orientation time series (κ^2) and compared them with the measured decay curves. The decay curves were emulated using the Markov chain[32] model presented in Figure 7 (top), which was shown to be the best approach for calculating fluorescence observables.[11h−k] Starting from the donor excited state (D*A), the probabilities of FRET (p_{FRET}), donor emission (p_D), and acceptor emission (p_A) were calculated for every saved snapshot of the MD trajectory according to

$$p_{FRET} = (1 - e^{-(k_D + k_{FRET})\Delta t})\frac{k_{FRET}}{k_D + k_{FRET}} \quad (7)$$

$$p_D = (1 - e^{-(k_D + k_{FRET})\Delta t})\frac{k_D}{k_D + k_{FRET}} \quad (8)$$

$$p_A = 1 - e^{-k_A\Delta t} \quad (9)$$

with Δt = 4 ps being the time step at which coordinates were saved, k_{FRET} the rate constant of energy transfer, $k_d = 1/\tau_D$ = 0.24 ns^{-1}, and $k_A = 1/\tau_A$ = 0.19 ns^{-1} the respective fluorescence rate constants of the donor and acceptor dyes. The rate constant of energy transfer k_{FRET} was calculated from

$$k_{FRET} = k_D\left(\frac{R_0(\kappa^2)}{R}\right)^6 \quad (10)$$

with R being the dye−dye distance d(B···B), and $R_0(\kappa^2)$ the dye−dye orientation-dependent Förster radius.[8] $R_0(\kappa^2)$ was calculated according to

$$R_0(\kappa^2) = R_0(2/3)\sqrt[6]{\frac{3}{2}\kappa^2} \quad (11)$$

The Förster radius R_0 (2/3) for κ^2 = 2/3 that is valid in case of freely rotating, isotropically averaged dyes was determined to be 4.91 nm. The orientation factor κ^2 was calculated according to[30]

$$\kappa^2 = (\cos\theta_{DA} - 3\cos\theta_D\cos\theta_A)^2 \quad (12)$$

with the angles defined by $\theta_{DA} = \angle(\vec{D},\vec{A})$,$\theta_D = \angle(\vec{D},\vec{R})$, and $\theta_A = \angle(\vec{A},\vec{R})$. The vectors $\vec{A}$ and $\vec{D}$ represent the emission transition dipole moment of the donor and the absorption transition dipole moment of the acceptor dye, respectively. $\vec{R}$ is the connection vector between the boron atoms of the dyes (Figure 7, bottom).

A total of 2500 different snapshots picked along regular intervals of 0.2 ns served as starting points for the Markov model. The model was started at state D*A and advanced by stepping through the trajectory. For every snapshot, transition probabilities according to eqs 7−9 were recalculated as functions of R and κ^2 (eqs 10−12). This process was stopped if photon emission from either the donor or the acceptor occurred or if the end of the trajectory was reached. The donor/acceptor photon counts at their respective emission times were summed up. To collect a statistically significant number of photon emission events, each of the 2500 runs was repeated 48 000 times to inject overall 120 millions of photons into each FRET emulation. The resulting decay curves were

dx.doi.org/10.1021/ja4104292 | J. Am. Chem. Soc. 2014, 136, 2441−2449

convolved with the respective IRFs to allow a direct comparison with experimental data.

The measured and emulated donor fluorescence emission decay curves of vase cavitand **1a** and kite cavitand **2** based on CGenFF trajectories are presented in Figure 8. When

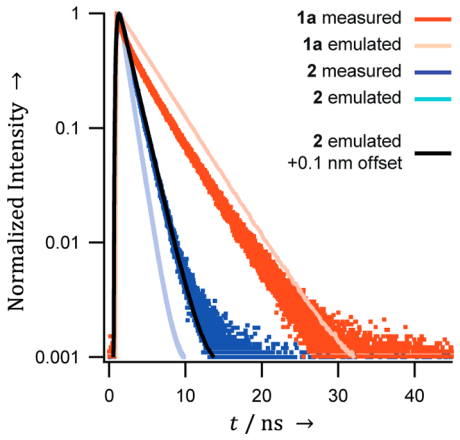

Figure 8. Measured and emulated donor fluorescence emission decay curves of vase cavitand **1a** (with an implemented donor-only fraction of 18%) and kite cavitand **2**.

performing the emulation of the donor decay in cavitand **1a** without taking a donor-only-labeled fraction into account, an extremely rapid decay is observed that basically parallels the IRF.[33] The experimentally observed donor decay curve can only be reproduced if a donor-only labeled fraction is taken into account. Thus, 100% FRET efficiency is indeed expected for vase cavitands **1a–d** due to the close dye–dye distance and should not be obscured by a possibly suboptimal orientation of transition dipole moments. The deviation between the emulated and the measured curves stems from the fast decay component in the experimental curve that we attribute to dynamic collisional quenching between the fluorophores. The effect of quenching at low dye–dye distances is not described by Förster theory and is therefore not taken into account in the FRET emulation.[11i]

In contrast, the emulated donor decay curve of kite cavitand **2** is close to the experimental result, albeit with a slightly shorter average lifetime (1.01 ns) than the measured curve (1.51 ns), suggesting that the MD simulation underestimates the average dye–dye distance to some extent, most probably because of a slight deviation in the kite opening angle. Indeed, emulation of the donor fluorescence intensity decay curve on the basis of a simulated dye–dye distance distribution that is shifted by +0.1 nm yielded excellent overlap with the measured curve (Figure 8). This deviation in the average distance of ~2% is in the same range as the difference between the results from the two force fields used (Figure 4) and illustrates the accuracy of MD simulations in reflecting the structural properties of molecular systems. With the information from the simulations, we can also test the accuracy of simple averaging regimes commonly used for analysis of FRET in dynamic systems.[11b,34] Since for cavitand **2** both the rotational correlation times of the dyes (Figure 6) and the distance dynamics between them (Figure 5) are much shorter than the fluorescence lifetimes, the system should be well approximated by the dynamic averaging regime, for which

$$\langle E \rangle = \frac{1}{1 + \left(\int (R_0/r)^6 P(r) \mathrm{d}r\right)^{-1}} \quad (13)$$

Using the distance distribution of cavitand **2** from the simulations shifted by 0.1 nm as described above, we obtain an average transfer efficiency, $\langle E \rangle$, of 68%. The fair agreement with the experimental value of 64% indicates that dynamic averaging is a reasonable approximation.

CONCLUSIONS

The distance distribution and dynamics between moieties attached to resorcin[4]arene cavitand walls in both the kite and the vase conformations have been studied by a combination of experimental and theoretical methods on the basis of BODIPY dye-substituted vase cavitands **1a–d** and kite cavitand **2**. In kite cavitand **2**, featuring one phenylene–ethynylene linker unit per dye, the dye moieties adopt an average distance of ca. 4.2 nm according to MD simulations (CGenFF). Time-resolved fluorescence spectroscopy revealed a FRET efficiency of 64%. In the case of vase cavitands **1a–d**, steady-state and time-resolved fluorescence spectroscopy showed increasing amounts of donor fluorescence for cavitands with longer arms. In early studies, this trend was explained by increasing dye–dye distances for cavitands with longer arms, which would be consistent with the presence of a nonzero cavitand opening angle. In the current study, we found according to MD simulations (CGenFF) that while the average dye–dye distance does indeed increase from 0.8 nm in the shortest cavitand **1c** to 1.2 nm in the longest cavitand **1a**, these distances are still in a range that should yield FRET efficiencies of 100%. Instead, the increasing donor fluorescence for cavitands with longer arms could be explained by the previously undetected presence of cavitand fractions with inactive acceptor components lacking the BF_2 unit. Emulation of the fluorescence intensity decay curve of cavitand **1a** from simulated MD trajectories confirmed that the experimentally observed decay curve can only be reproduced when a donor-only-labeled cavitand fraction is taken into account.

The dynamics of vase cavitand **1a** was investigated by fluorescence anisotropy measurements. Evaluation of both measured and simulated fluorescence anisotropy decay curves showed that the rotation time of a BODIPY dye arm in cavitand **1a** is ca. 0.15 ns. Autocorrelation analysis of the dye–dye distance time series revealed that the distance dynamics of the BODIPY dye arms takes place on the subnanosecond time scale. Most importantly, the fluorescence lifetime decays calculated based on the MD simulations of cavitand **2** are in excellent agreement with the experimental data, showing that the simulations present an accurate picture of the distance distribution and dynamics in this molecular system. With these results, the cavitand system can now be used as a platform to investigate fundamental, distance-dependent interactions between objects attached to the cavitand's walls.

In the case of extended molecular and supramolecular systems with pronounced flexibility and therefore broad intramolecular distance distributions, the combination of time-resolved FRET with simulations is essential to quantify the underlying dynamics because the experimental observables depend on both the shape of the distance distribution and the time scale of the dynamics. In this work, we have in-depth structurally characterized the two conformational states of resorcin[4]arene cavitands, which opens the possibility to utilize the cavitand system for studying intraspace interactions

dx.doi.org/10.1021/ja4104292 | J. Am. Chem. Soc. 2014, 136, 2441–2449

ranging from 1 to 7 nm (adjustable via the linker length). Furthermore, the good agreement between MD simulations and experimental data should further encourage application of MD simulations to molecular chemical systems. Progress in force-field development now allows such simulations to be performed with high accuracy. MD simulations could serve as a testing tool for envisioned concepts and thereby guide the synthetic chemist toward successful implementation of his/her ideas.

Although the dyes used in this study are not suitable for single-molecule fluorescence detection, an approach analogous to the one demonstrated here could be employed for single-molecule studies. Such experiments could further enhance the resolution of structural and dynamic heterogeneities in molecular systems.

■ ASSOCIATED CONTENT

Supporting Information

Synthetic procedures, characterization data, X-ray data, fluorescence data, MD methods, NMR spectra. This material is available free of charge via the Internet at http://pubs.acs.org.

■ AUTHOR INFORMATION

Corresponding Authors

caflisch@bioc.uzh.ch
schuler@bioc.uzh.ch
diederich@org.chem.ethz.ch

Notes

The authors declare no competing financial interest.

■ ACKNOWLEDGMENTS

This work was supported by grants from the Swiss National Science Foundation (SNF). I.P. acknowledges the receipt of a fellowship from the Fonds der Chemischen Industrie. Research was partly carried out in the Laser Resource Center of the Beckman Institute of the California Institute of Technology and supported by the Arnold and Mabel Beckman Foundation. We thank Prof. Dr. Gunnar Jeschke, Dr. Marc-Olivier Ebert, and Dr. Andreas Vitalis for helpful discussions, Dimitry Kotlyar for help with the Table of Contents artwork, and Dr. Kenno Vanommeslaeghe for providing parametrization of the cavitands via the Paramchem engine.

■ REFERENCES

(1) (a) Moran, J. R.; Ericson, J. L.; Dalcanale, E.; Bryant, J. A.; Knobler, C. B.; Cram, D. J. *J. Am. Chem. Soc.* **1991**, *113*, 5707. (b) Moran, J. R.; Karbach, S.; Cram, D. J. *J. Am. Chem. Soc.* **1982**, *104*, 5826.

(2) Skinner, P. J.; Cheetham, A. G.; Beeby, A.; Gramlich, V.; Diederich, F. *Helv. Chim. Acta* **2001**, *84*, 2146.

(3) (a) Frei, M.; Marotti, F.; Diederich, F. *Chem. Commun.* **2004**, 1362. (b) Durola, F.; Rebek, J., Jr. *Angew. Chem., Int. Ed.* **2010**, *49*, 3189.

(4) (a) Berryman, O. B.; Sather, A. C.; Lledo, A.; Rebek, J. *Angew. Chem., Int. Ed.* **2011**, *50*, 9400. (b) Berryman, O. B.; Sather, A. C.; Rebek, J., Jr. *Chem. Commun.* **2010**, *47*, 656.

(5) Pochorovski, I.; Boudon, C.; Gisselbrecht, J.-P.; Ebert, M.-O.; Schweizer, W. B.; Diederich, F. *Angew. Chem., Int. Ed.* **2012**, *51*, 262.

(6) Pochorovski, I.; Ebert, M.-O.; Gisselbrecht, J.-P.; Boudon, C.; Schweizer, W. B.; Diederich, F. *J. Am. Chem. Soc.* **2012**, *134*, 14702.

(7) (a) Barboiu, M.; Lehn, J.-M. *Proc. Natl. Acad. Sci. U.S.A.* **2002**, *99*, 5201. (b) Dietrich-Buchecker, C. O.; Jimenez-Molero, M. C.; Sartor, V.; Sauvage, J. P. *Pure Appl. Chem.* **2003**, *75*, 1383. (c) Azov, V. A.; Schlegel, A.; Diederich, F. *Angew. Chem., Int. Ed.* **2005**, *44*, 4635. (d) Azov, V. A.; Beeby, A.; Cacciarini, M.; Cheetham, A. G.; Diederich, F.; Frei, M.; Gimzewski, J. K.; Gramlich, V.; Hecht, B.; Jaun, B.; Latychevskaia, T.; Lieb, A.; Lill, Y.; Marotti, F.; Schlegel, A.; Schlittler, R. R.; Skinner, P. J.; Seiler, P.; Yamakoshi, Y. *Adv. Funct. Mater.* **2006**, *16*, 147. (e) Wu, J.; Leung, K. C.-F.; Benítez, D.; Han, J.-Y.; Cantrill, S. J.; Fang, L.; Stoddart, J. F. *Angew. Chem., Int. Ed.* **2008**, *47*, 7470.

(8) Förster, T. *Ann. Phys. (Berlin, Ger.)* **1948**, *2*, 55.

(9) Azov, V. A.; Schlegel, A.; Diederich, F. *Bull. Chem. Soc. Jpn.* **2006**, *79*, 1926.

(10) Pochorovski, I.; Breiten, B.; Schweizer, W. B.; Diederich, F. *Chem.—Eur. J.* **2010**, *16*, 12590.

(11) (a) Gustiananda, M.; Liggins, J. R.; Cummins, P. L.; Gready, J. E. *Biophys. J.* **2004**, *86*, 2467. (b) Schuler, B.; Lipman, E. A.; Steinbach, P. J.; Kumke, M.; Eaton, W. A. *Proc. Natl. Acad. Sci. U.S.A.* **2005**, *102*, 2754. (c) Merchant, K. A.; Best, R. B.; Louis, J. M.; Gopich, I. V.; Eaton, W. A. *Proc. Natl. Acad. Sci. U.S.A.* **2007**, *104*, 1528. (d) Best, R. B.; Merchant, K. A.; Gopich, I. V.; Schuler, B.; Bax, A.; Eaton, W. A. *Proc. Natl. Acad. Sci. U.S.A.* **2007**, *104*, 18964. (e) Corry, B.; Jayatilaka, D. *Biophys. J.* **2008**, *95*, 2711. (f) Unruh, J. R.; Kuczera, K.; Johnson, C. K. *J. Phys. Chem. B* **2009**, *113*, 14381. (g) Schuetz, P.; Wuttke, R.; Schuler, B.; Caflisch, A. *J. Phys. Chem. B* **2010**, *114*, 15227. (h) Liao, J.-M.; Wang, Y.-T.; Chen, C.-L. *Phys. Chem. Chem. Phys.* **2011**, *13*, 10364. (i) Hoefling, M.; Lima, N.; Haenni, D.; Seidel, C. A. M.; Schuler, B.; Grubmüller, H. *PLoS ONE* **2011**, *6*, e19791. (j) Speelman, A. L.; Muñoz-Losa, A.; Hinkle, K. L.; VanBeek, D. B.; Mennucci, B.; Krueger, B. P. *J. Phys. Chem. A* **2011**, *115*,, 3997;. (k) Hoefling, M.; Grubmüller, H. *Comput. Phys. Commun.* **2013**, *184*, 841.

(12) Azov, V. A.; Jaun, B.; Diederich, F. *Helv. Chim. Acta* **2004**, *87*, 449.

(13) A more detailed discussion on the instability of the acceptor dye is provided in section 1.4 of the Supporting Information.

(14) (a) Liras, M.; Prieto, J. B.; Pintado-Sierra, M.; Arbeloa, F. L.; García-Moreno, I.; Costela, Á.; Infantes, L.; Sastre, R.; Amat-Guerri, F. *Org. Lett.* **2007**, *9*, 4183. (b) Bañuelos, J.; López Arbeloa, F.; Arbeloa, T.; Salleres, S.; Vilas, J. L.; Amat-Guerri, F.; Liras, M.; López Arbeloa, I. *J. Fluoresc.* **2008**, *18*, 899.

(15) (a) Crawford, S. M.; Thompson, A. *Org. Lett.* **2010**, *12*, 1424. (b) Smithen, D. A.; Baker, A. E. G.; Offman, M.; Crawford, S. M.; Cameron, T. S.; Thompson, A. *J. Org. Chem.* **2012**, *77*, 3439.

(16) Published in ref 10.

(17) For details, see section 2 of the Supporting Information.

(18) There are no indications that electron transfer, neither between the two dyes nor between the dyes and the quinone walls, significantly affects the transfer dynamics. For a more detailed discussion, see section 3.2 of the Supporting Information.

(19) Meer, B. W. V. d.; Coker, G.; Chen, S.-Y. S. *Resonance Energy Transfer: Theory and Data*; VCH Publishers, Inc.: New York, 1994.

(20) For details, see Figure S5 in section 3.1 of the Supporting Information.

(21) An analyis of the decay curves is provided in section 3.4 of the Supporting Information.

(22) (a) Karolin, J.; Johansson, L. B.-Å.; Strandberg, L.; Ny, T. *J. Am. Chem. Soc.* **1994**, *116*, 7801. (b) Bergström, F.; Hägglöf, P.; Karolin, J.; Ny, T.; Johansson, L. B.-Å. *Proc. Natl. Acad. Sci. U.S.A.* **1999**, *96*, 12477. (c) Bergström, F.; Mikhalyov, I.; Hägglöf, P.; Wortmann, R.; Ny, T.; Johansson, L. B.-Å. *J. Am. Chem. Soc.* **2002**, *124*, 196. (d) Mikhalyov, I.; Gretskaya, N.; Bergström, F.; Johansson, L. B.-Å. *Phys. Chem. Chem. Phys.* **2002**, *4*, 5663. (e) Tleugabulova, D.; Zhang, Z.; Brennan, J. D. *J. Phys. Chem. B* **2002**, *106*, 13133.

(23) (a) Fischer, S.; Grootenhuis, P. D. J.; Groenen, L. C.; van Hoorn, W. P.; van Veggel, F. C. J. M.; Reinhoudt, D. N.; Karplus, M. *J. Am. Chem. Soc.* **1995**, *117*, 1611. (b) den Otter, W. K.; Briels, W. J. *J. Am. Chem. Soc.* **1998**, *120*, 13167. (c) Tolpekina, T. V.; den Otter, W. K.; Briels, W. J. *J. Phys. Chem. B* **2003**, *107*, 14476. (d) Casanovas, J.; Zanuy, D.; Aleman, C. *Angew. Chem., Int. Ed.* **2006**, *45*, 1103. (e) Ewell, J.; Gibb, B. C.; Rick, S. W. *J. Phys. Chem. B* **2008**, *112*, 10272. (f) Javor, S.; Rebek, J. *J. Am. Chem. Soc.* **2011**, *133*, 17473. (g) Cézard, C.; Trivelli, X.; Aubry, F.; Djedaïni-Pilard, F.; Dupradeau, F.-Y. *Phys. Chem. Chem. Phys.* **2011**, *13*, 15103. (h) Zhang, H.; Tan, T.;

Feng, W.; van der Spoel, D. *J. Phys. Chem. B* **2012**, *116*, 12684. (i) Zheng, X.; Wang, D.; Shuai, Z.; Zhang, X. *J. Phys. Chem. B* **2012**, *116*, 823. (j) Simona, F.; Nussbaumer, A. L.; Häner, R.; Cascella, M. *J. Phys. Chem. B* **2013**, *117*, 2576.
(24) (a) Wang, J.; Wolf, R. M.; Caldwell, J. W.; Kollman, P. A.; Case, D. A. *J. Comput. Chem.* **2004**, *25*, 1157. (b) Vanommeslaeghe, K.; Hatcher, E.; Acharya, C.; Kundu, S.; Zhong, S.; Shim, J.; Darian, E.; Guvench, O.; Lopes, P.; Vorobyov, I.; Mackerell, A. D., Jr. *J. Comput. Chem.* **2009**, *31*, 672.
(25) (a) Wang, J.; Wang, W.; Kollman, P. A.; Case, D. A. *J. Mol. Graph. Model.* **2006**, *25*, 247. (b) Vanommeslaeghe, K.; Mackerell, A. D., Jr. *J. Chem. Inf. Model.* **2012**, *52*, 3144. (c) Vanommeslaeghe, K.; Raman, E. P.; Mackerell, A. D., Jr. *J. Chem. Inf. Model.* **2012**, *52*, 3155.
(26) (a) van der Spoel, D.; van Maaren, P. J.; Caleman, C. *Bioinformatics* **2012**, *28*, 752. (b) Caleman, C.; van Maaren, P. J.; Hong, M.; Hub, J. S.; Costa, L. T.; van der Spoel, D. *J. Chem. Theory Comput.* **2012**, *8*, 61.
(27) For details, see section 4 of the Supporting Information.
(28) (a) Godt, A.; Schulte, M.; Zimmermann, H.; Jeschke, G. *Angew. Chem., Int. Ed.* **2006**, *45*, 7560. (b) Jeschke, G.; Sajid, M.; Schulte, M.; Ramezanian, N.; Volkov, A.; Zimmermann, H.; Godt, A. *J. Am. Chem. Soc.* **2010**, *132*, 10107.
(29) Dunn, P. F. *Measurement and Data Analysis for Engineering and Science*; McGraw-Hill: New York, 2005.
(30) Lakowicz, J. R. *Principles of Fluorescence Spectroscopy*, 2nd ed.; Kluwer Academic/Plenum Publishers: New York, 1999.
(31) Lipari, G.; Szabo, A. *Biophys. J.* **1980**, *30*, 489.
(32) Norris, J. R. *Markov Chains*; University of Cambridge: Cambridge, 1998.
(33) See Figure S9 in section 5 of the Supporting Information.
(34) (a) Schuler, B.; Müller-Späth, S.; Soranno, A.; Nettels, D. *Methods Mol. Biol.* **2012**, *896*, 21. (b) Wozniak, A. K.; Schröder, G. F.; Grubmüller, H.; Seidel, C. A. M.; Oesterhelt, F. *Proc. Natl. Acad. Sci. U.S.A.* **2008**, *105*, 18337.